



## First gaseous boronization during pulsed discharge cleaning

J. Ko<sup>\*</sup>, D.J. Den Hartog, J.A. Goetz, P.J. Weix, S.T. Limbach

Department of Physics, University of Wisconsin, Madison, WI, USA

### ARTICLE INFO

#### Article history:

Received 28 December 2011

Accepted 26 July 2012

Available online 21 August 2012

### ABSTRACT

The first successful gaseous boronization during a pulsed discharge is reported. Sublimation of *o*-carborane ( $C_2B_{10}H_{12}$ ) combined with pulsed discharge plasmas with a repetition rate of 1 Hz is used to produce a hard boron-containing coating for reversed field pinch (RFP) plasmas in the Madison Symmetric Torus. X-ray photoelectron spectroscopy with Ar ion beam etching for silicon coupons installed at the plasma boundary shows about 60% boron concentration in the deposited layer. Both profilometer and scanning electron microscope analyses of the silicon coupons imply a strong toroidally non-uniform deposition depending on the location of the *o*-carborane injection. The layer thickness ranges from 50 to 300 nm. Ellipsometry calibrated with the profilometer results yields a refractive index of 2.2–2.3 for the films. The high refractive index implies that the coating is hard and has a well-ordered morphology. A reduction in wall recycling has consistently been observed after all boronization sessions. Comparison of the X-ray spectra in standard RFP plasmas before and after boronization indicates a slight decrease in the effective ionic charge.

© 2012 Elsevier B.V. All rights reserved.

### 1. Introduction

Coating the vacuum vessel wall with low-atomic-number materials has become an essential part in many present magnetic-confinement fusion experiments to reduce the interactions of the plasma particles and the impurities with the wall material in addition to improving the vacuum condition by gettering oxygen [1]. Many contemporary devices use boronization for the wall coating, as it has been seen to improve plasma performance [2]. Various boron compounds have been used for boronization including diborane ( $B_2H_6$  or  $B_2D_6$ ) [2], trimethylboron ( $B(CH_3)_3$  or  $B(CD_3)_3$ ) [3], decarborane ( $B_{10}H_{14}$  or  $B_{10}D_{14}$ ) [4], and *o*-carborane ( $C_2B_{10}H_{12}$ ) [5]. Most of these substances, except decarborane and *o*-carborane, are toxic and explosive and therefore, require additional and substantial safety resources to carry out the boronization. Techniques using *o*-carborane are relatively safe and easy compared with the rest of the methods and the recent ‘brand-new’ fusion devices also have adopted the *o*-carborane method [6,7]. The safe and simple nature of the *o*-carborane technique makes it the most appropriate to the Madison Symmetric Torus (MST) since the device resides in a university building with hundreds of students coming and going daily and the boundary between the machine area and the rest of the building is not gas-sealed.

Usually, *o*-carborane powder is sublimated at 70–150 °C and injected into a glow discharge plasma that decomposes the gaseous *o*-carborane molecules. One big challenge at MST is that the

decomposing discharge is pulsed. The gap between the top and bottom ‘half’ torus-shape vacuum vessels of MST is viton-sealed and the cables for the magnetic coil arrays are in the pumping duct which is separated by 252 holes of 3.8 cm in diameter from the main plasma chamber above it. The glow plasma could easily contact and damage the viton at the gap and once the glow penetrates into the pumping duct through the holes, it could damage the magnetic array cables. For these reasons, glow discharges are not allowed in MST. The prohibition of glow discharge is not favorable for boronization in terms of cost and time because pulsing the discharge will decrease the chance for the boron-carrying molecules and the plasma to react with each other.

However, recent *o*-carborane sublimation tests for the MST vacuum system imply that the residence time of the *o*-carborane molecules and their cracks is longer by an order of magnitude than expected based on the pumping speed and the chamber volume. These observations motivate boronization experiments with a pulsed discharge at MST. Section 2 describes the pulsed discharge and boronization procedures, followed by the characteristics of the boron-containing films and the effects on the reversed field pinch (RFP) plasmas (Section 3). Finally, the summary and discussion are given in Section 4.

### 2. Experimental setup

#### 2.1. Pulsed discharge cleaning

MST is a mid-size RFP device with major and minor radii of 1.5 m and 0.52 m, respectively. The plasmas typically have plasma

<sup>\*</sup> Corresponding author. Tel.: +82 42 879 5164.

E-mail address: [jinseok@nfri.re.kr](mailto:jinseok@nfri.re.kr) (J. Ko).

current ( $I_p$ )  $\leq 600$  kA, magnetic field ( $B$ )  $\leq 0.7$  T, electron density ( $n_e$ )  $\leq 2 \times 10^{19}$  m $^{-3}$ , electron and ion temperatures ( $T_e$  and  $T_i$ )  $\leq 2$  keV, and a pulse length of 60 ms. The vertical equilibrium field is provided by the image currents inside the 50 mm thick, high-conductivity aluminum (6061-T6) vacuum vessel wall. The MST vacuum vessel has no liner and therefore, aluminum is the main plasma facing component with a small portion (about 10%) of the wall covered with graphite and ceramic limiters. During RFP experimental sessions, three turbo pumps and two cryopumps are in operation. Each turbo pump has a pumping speed of 1000 l/s. One cryopumps out nitrogen, water, hydrogen and helium with the speeds of 1000, 4000, 1000, and 1000 l/s, respectively, while the other only works for nitrogen and water with the speeds of 1000 and 4000 l/s, respectively. These maintain the MST vessel baseline pressure down to about  $5 \times 10^{-7}$  Torr.

MST routinely conditions its walls every night with a helium pulsed discharge cleaning (PDC) – a variation of Taylor discharge cleaning [8] – with a typical repetition rate of 0.2 Hz (2–3 ms discharge every 5 s). A separate power supply is used for PDC and it has been modified for boronization purposes to increase the repetition rate. This is done by reducing the number of capacitors that energize the toroidal and poloidal field coils and by reducing the capacitor charging time. Thus far, 1 Hz has been achieved with this modification. The discharge parameters including the plasma current, density, etc. change accordingly. Fig. 1 compares  $I_p$ ,  $T_e$  measured by a Langmuir probe,  $n_e$  measured by a far-infrared interferometer, and neutral pressure measured by a fast ion gauge between the ‘normal’ 0.2 Hz (for the routine overnight wall conditioning) and ‘fast’ 1 Hz (for the boronization) PDCs. During PDC sessions, the cryopump that removes hydrogen, helium, nitrogen and water is isolated from the vacuum chamber, so that the working gas (helium) is effectively being pumped by the turbo pumps only. It is noted that even the reduced  $I_p$  ( $\approx 10$  kA) with the fast PDC is still much larger than those from typical glow discharges that are used for the o-carborane boronization in other devices ( $\leq 2$  A) [5,9].

## 2.2. Boronization

In previous efforts to boronize the vacuum vessel at MST, a solid B $_4$ C rod inserted into the vessel at one toroidal location was used. The rod was eroded by the interaction with the plasma particles to form an a-B/C:H film on the surface during standard RFP discharges [10] or a normal PDC session [11]. Although there was a reduction of the low-charge-state impurity radiation, this approach had

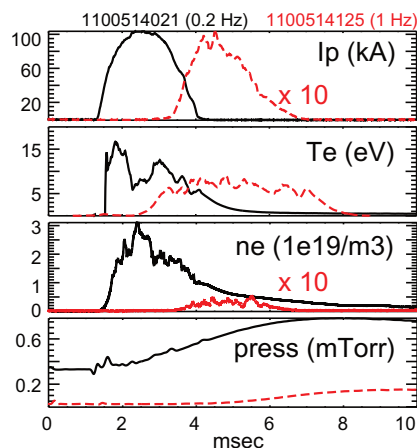


Fig. 1. Comparison of plasma current ( $I_p$ ), electron temperature ( $T_e$ ), electron density ( $n_e$ ), and neutral pressure (from the top to the bottom) between the normal (0.2 Hz, solid) and fast (1 Hz, dashed) PDCs.  $I_p$  and  $n_e$  from the fast PDC (1100514125) have been multiplied by 10 for easy comparison.

difficulty controlling the amount and having uniformity in the coating and was simply too cumbersome to operate routinely.

To date, the gaseous approach has been attempted using o-carborane sublimation and deposition assisted by 1 Hz helium pulsed discharges. An o-carborane ‘oven’ consists of a container typically loaded with 7 g of o-carborane powder, an elbow-shape nipple, a gas shut-off valve, and a gate valve to the MST main chamber. The oven is connected to the outside of the vacuum vessel in a radial direction near the midplane. The total transmission of o-carborane is less than 20 cm long. The oven is pre-pumped down to a few mTorr through a pumping system which is separate from the main MST pumping system before the gate valve is opened to the MST main chamber ( $5 \times 10^{-7}$ ). Fig. 2 shows a picture of the oven attached to the MST chamber, showing the components described above. Multiple heating ropes are applied to all the oven components, including the gate valve, to avoid o-carborane condensation. Some parts of the oven had experienced condensation in earlier attempts when the heating was not provided thoroughly to the system. The most recent heating configuration controls the temperature at five different locations to guarantee spatial uniformity in temperature and to avoid overshoot during the temperature ramp-up phase at the beginning of the heating. To minimize the heat loss to the atmosphere, the oven is wrapped with fiberglass insulating ropes. With these heating and control systems, the temperature can be maintained to be 80–85 °C over the entire injection system for more than three hours. The entire MST vacuum vessel does not have to be heated with the same temperature as the o-carborane oven. The MST vessel is usually maintained at room temperature. Inspections done during maintenance vents (done usually several weeks after the boronization event) have verified no massive o-carborane condensation exists on the MST wall even near the injection port. The inspection also confirms there is no condensation in the pumping system that may cause clogging of the pumping lines.

Two silicon coupons ( $1.5 \times 1.5$  cm $^2$ ) are used to enable study of the characteristics of the coating. The coupons are installed at the end of insertable probes that are positioned flush with the MST inner wall. A residual gas analyzer (RGA) is used to monitor the partial pressures of the sublimated o-carborane and other gaseous molecules such as hydrogen, oxygen, and water. Fig. 3 lays out the locations of the Si coupons along with those of the pumps described in Section 2.1, the RGA, and the two o-carborane ovens (used separately) for the boronization experiments.

A typical boronization experiment includes two RFP plasma sessions before and after the boronization to estimate the boronization effects. This experiment is outlined here. The pre-boronization plasma session consists of 40–50 standard RFP plasma discharges. In these discharges we use the far-infrared interferometer to

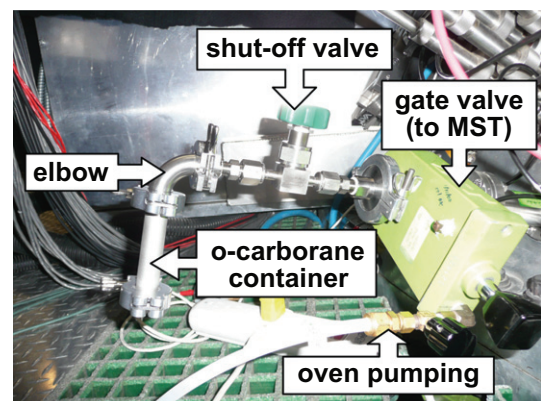
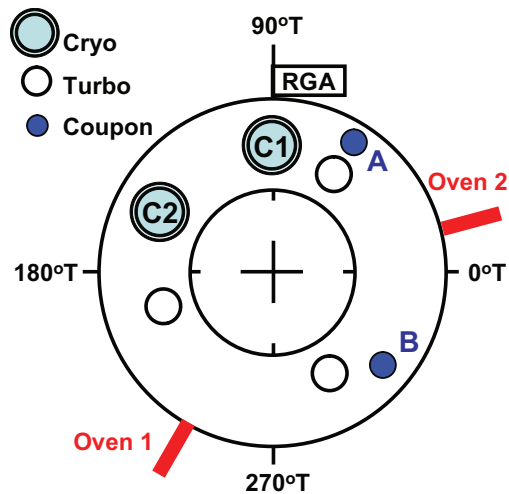


Fig. 2. A picture of the oven attached to the MST main chamber. The picture was taken before the heating and insulating ropes were applied.



**Fig. 3.** Top view of the MST chamber showing the layouts of the Si coupons (A and B), RGA, two cryopumps (C1 and C2), three turbo pumps, and two o-carborane ovens (used in separate experiments). The cryopump 2 (C2) is usually turned off during the PDC. “T” at the end of the coordinate angles stands for the toroidal location. The pumps and RGA are attached to the bottom of the torus, the coupons to the top, and the ovens at the midplane.

measure the density, the X-ray spectrometer to measure the relative change in the effective ionic charge ( $Z_{\text{eff}}$ ), and impurity monochromator arrays (IMA) to measure low-charge-state-impurity line radiations such as BIV, CV, OIV and NIV. Then, the boronization PDC is performed with the coupons inserted. It takes about 3 h for all of the o-carborane powder ( $\sim 7$  g) in the oven to be sublimated away. The mass 70 (from one of the o-carborane cracks) is observed during the boronization with the RGA. The oven is open to the chamber without the plasma first. Several minutes after the oven heating is applied, the mass 70 signal increases gradually. When the gradient of the increase is reduced near the equilibration point between the supply of the o-carborane and the amount leaving the chamber, the PDC is turned on. As soon as the PDC is turned on, the o-carborane signal rapidly drops, but after a while, the o-carborane level reaches another equilibration (about 10–20% the background level) and maintains it over the course of the PDC session – this time a balance among the supply, the decomposition by the plasma, and pumping out. The entire consumption of the o-carborane is assured by temporarily turning off the PDC to see if the o-carborane signal in the RGA increases without the discharge. If it does, the PDC resumes and this checking procedure is repeated until the o-carborane signal shows no change. The boronization PDC session is followed by the normal (0.2 Hz) overnight PDC to remove excessive hydrogen that is from the o-carborane molecules. Finally, another RFP plasma session is done with the same number of shots and the same diagnostics. The coupons are taken out from MST before this last RFP session and delivered to a local materials science center for a variety of materials analyses such as X-ray photoelectron spectroscopy (XPS), ellipsometry, profilometry, and scanning electron microscopy (SEM). The following section discusses the deposition characteristics gleaned from these materials analyses and the plasma performance from the diagnostics for the plasmas before and after the boronization.

### 3. Results

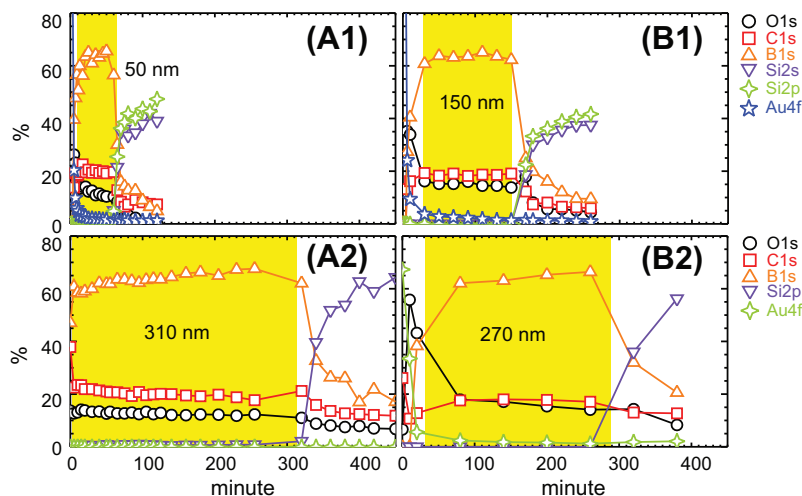
#### 3.1. Sample analysis

Two small vacuum-compatible carbon masks are applied to two corners of the Si coupon before it is inserted into the MST vessel so that a sharp step on the surface is available for the profilometer

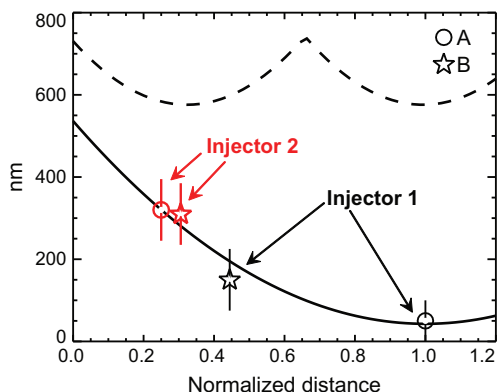
measurement. The coupons after the boronization test are transferred to a vacuum cavity which maintains the coupons in low vacuum ( $\leq 10$  mTorr) before they are taken out for the materials tests. The first test is the ellipsometer from which one can get a set of combinations of the thickness and refractive index of the film depending on the initial values the user inputs. This is followed by the profilometer test where it is necessary to coat the coupon surface with a conducting material (usually, gold) since the Si coupon and the boron-carbon deposition on it are not conducting enough for the light from the profilometer to polarize the surface effectively. The 20 nm gold sputtering turns out to produce reasonable profilometer measurements. Finally, the depth profile of the coupon is measured with XPS and  $\text{Ar}^+$  beam etching. The etching rate is estimated to be 1 nm/min for the B/C film based on the profilometer measurement. Alternatively, the SEM can be performed before the XPS measurement.

Fig. 4 shows the depth profiles of the films obtained from two boronization experiments which have different o-carborane injection locations. A1 and B1 denote the Si coupons A and B with injector 1 and A2 and B2 with injector 2 (See Fig. 3 for their locations). It is noted that all the coupons have 60–70% of boron concentration and the ratio of boron and carbon is about 3:1 which is close to their initial composition of the source (5:1). Oxygen is also constantly embedded inside the B/C film, implying that oxygen gettering is taking place during the formation of the film. The oxygen level drops near the boundary of the film and the Si substrate. Note, however, that the constant level of oxygen (15–20%) throughout the B/C film also implies that there might be a constant source of oxygen or water vapor. Recent calculations estimate the permeation rates through the flat Viton gaskets (for the vacuum vessel sealing) and the TPX windows (for the far-infrared polarimeter/interferometer (FIR) system) can be up to  $3 \times 10^{-4}$  Torr l/s for oxygen and water vapor. The solutions to these leaks such as replacement of windows and differentially-pumped gaskets are under consideration. The sputtered gold (Au4f) is quickly removed at the early stage of the beam etching, thus estimating an etching rate of 3–4 nm/min, and does not affect the depth profiling of the film at all. It is also noted that according to the XPS depth profiles, there is no aluminum line observed throughout the film formation which is somewhat different from what is expected since aluminum is the majority plasma-facing material at MST. In this sense, this is also the first demonstration that there is no strong plasma-wall interaction during the PDC. The thickness of the coating significantly depends on the location of the o-carborane injection. While the coupon farthest away from the injector (A1 in Fig. 4) has only 50 nm coating, the coupons near the injector (A2 and B2 in Fig. 4) have about 300 nm. From these measurements, one can roughly estimate the expected deposition profile along the toroidal direction, which is shown in Fig. 5 where a parabolic fit is done for the film thickness and the distance between the o-carborane source and the coupon in the toroidal direction. This scaling can provide a guideline on how many injectors are needed to achieve uniformity in the deposition. For example, three injectors evenly distributed in the toroidal direction should suffice in order to obtain about 600–750 nm uniform coating.

Other analyses complement and confirm the XPS measurements. Once the thickness measurements from the XPS and profilometer confirm each other, the ellipsometer measurements are revisited and the right combination of initial thickness and refractive index can be chosen. Table 1 summarizes the thicknesses measured by these three instruments for the coupons whose XPS data are shown in Fig. 4. As shown in this summary, the measured thicknesses are in a good agreement among the instruments. Table 1 also contains the refractive index of the coating that is inferred by the ellipsometer. This high refractive index implies that the coating is hard and has a well-ordered morphology [7].



**Fig. 4.** XPS depth profiles with Ar<sup>+</sup> beam etching for the Si coupons from two different boronization experiments using the o-carborane injectors 1 and 2, respectively. For example, A1 indicates the coupon A with injector 1 (see Fig. 3 for the locations). One minute etching corresponds to 1 nm in depth. Shaded regions roughly indicate the thickness of the bulk B/C films.



**Fig. 5.** Experimental scaling of the film thickness in the toroidal direction from the measurements shown in Fig. 4. Normalized distance is the distance between the coupon and the o-carborane source divided by the toroidal half circumference of MST. In this parabolic fit (the goodness of the fit  $\chi^2 = 1.3$ ), it is assumed that the other toroidal half circumference has the same deposition pattern. The dashed line indicates the deposition profile expected with three evenly distributed ovens.

**Table 1**

Comparison of thicknesses measured by three instruments for the boronization coupons. Ellipsometer data also include the refractive index of the coating (in the parentheses).

Coupon	Instrument	Oven (o-carborane)	
		1 (7.2 g)	2 (6.0 g)
A	XPS	50	310
	Profilometer	67	313
	Ellipsometer	65 (2.3)	N/A
B	XPS	150	270
	Profilometer	163	290
	Ellipsometer	155 (2.2)	N/A

It is noted that the coating is much thicker than expected based on the duty cycle of the PDC (2 ms/1 s = 0.2%) assuming the deposition only takes place during discharges. Then, this low duty cycle would have only 0.2% out of the initial o-carborane loading participate in the film formation. This corresponds to about 0.7 nm homogeneous coating for the MST inner wall (30.8 m<sup>2</sup>) with 7 g of initial loading. However, the coating thickness we obtain is

50–300 nm and this is equivalent to using about 40% of the initial loading on average. It is speculated that this high ‘fuel’ efficiency against the low duty cycle of the PDC is due to the longer residence time of the o-carborane molecules and their cracks in the MST chamber. In o-carborane-into-vacuum tests where the o-carborane is injected into the vacuum vessel without plasmas and pumped out by the MST main pumping system, it is observed that after the oven valve is shut off, the partial pressure of the o-carborane decays with a characteristic time much slower than that calculated by the MST vessel volume (8 m<sup>3</sup>) and manufacturer-specified pumping speeds which should be in the order of several seconds. The exponential fit for the decay is expressed by two characteristic time constants: the shorter time constant (~3 min) which represents the ‘real’ residence time determined by the vessel volume and the real pumping speed and the longer time constant (7–8 min) which may represent slow outgassing of the condensed (and sticky) o-carborane from the rough aluminum wall.

### 3.2. Plasma performance

The RFP plasmas taken before and after the boronization are compared with each other in terms of impurity reduction and density control. Standard RFP discharges are subject to the global  $m = 1$  tearing instability, where  $m$  is the poloidal magnetic mode number, due to the intrinsically low safety factor across the plasma. This causes magnetic reconnection and relaxation of the current density profile. However, the profile experiences a critical gradient due to current profile peaking which again results in the tearing instability. Standard RFP discharges are sustained by the competition between these two processes [12]. This competition manifests itself in the form of quasi periodic sawtooth-like oscillation in a variety of global (and local) quantities such as toroidal flux. By ensembling many of these oscillation events and taking the average of the plasma quantities (measured by the stationary diagnostics) over the ensemble, one can effectively obtain flux-surface-averaged values for those quantities. The averaged values are centered at the sawtooth ‘crash’ time when the current density profile reaches its critical gradient and when the current profile peaking is overwhelmed by the tearing mode.

Some noticeable reduction in impurity radiation is observed after the boronization from this ‘sawtooth-ensemble’ analysis. Fig. 6 compares a few of the impurity line radiation signals, including one from boron measured by IMA from the sawtooth-ensemble

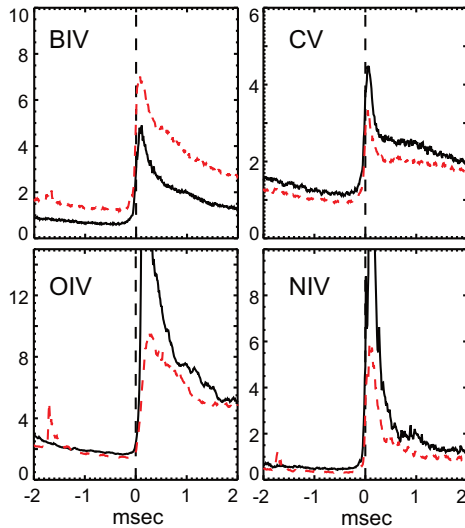


**Fig. 6.** Ensemble-averaged impurity line radiation before (solid) and after (dotted) the boronization. Time equal to 0 corresponds to the sawtooth crash and the vertical unit is arbitrary. The wavelengths are 282.17 nm for BIV, 227.09 nm for CV, 338.55 nm for OIV, and 347.87 nm for NIV.

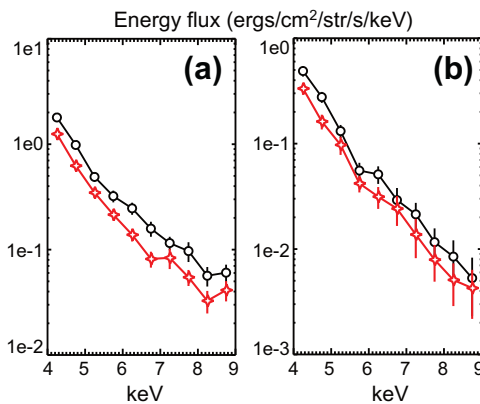


**Fig. 7.** Ensemble-averaged soft X-ray spectra from detector 2 (central viewing) at 0.5 ms before (a) and after (b) the sawtooth crash for the same plasma sets shown in Fig. 6. 46 spectra are averaged for the pre-boronization plasmas (circle) and 77 for the post-boronization plasmas (star).

analyses for the plasmas before (27 events) and after (51 events) the boronization. While the boron signal increases by a factor  $\leq 2$ , the rest of the impurities decrease by a similar factor after the boronization.

The IMA analysis is limited to low-charge-state impurity radiation which takes place mainly near the boundary of the plasma where the temperature is low. For example, there is no information on the high-charge-state of fully-stripped aluminum, one of the dominant impurities in MST. Also there can be other impurities with higher charge states at the core region of the plasma. One way to indirectly infer  $Z_{\text{eff}}$ , a more appropriate quantity that reflects the total amount of impurities, is to observe the X-ray spectra. With the assumption of the same temperature and density, the energy flux of the X-ray spectrum is proportional to  $Z_{\text{eff}}$  [13]. Fig. 7 shows the comparison of the ensemble-averaged soft X-ray spectra from the viewing chord that goes through the magnetic axis for the same discharge sets shown in Fig. 6. Although additional modeling is needed to quantify  $Z_{\text{eff}}$  with known plasma temperature and density, this result implies a relative decrease in  $Z_{\text{eff}}$  and therefore, overall decrease in the impurity content during the entire sawtooth cycle after the boronization.

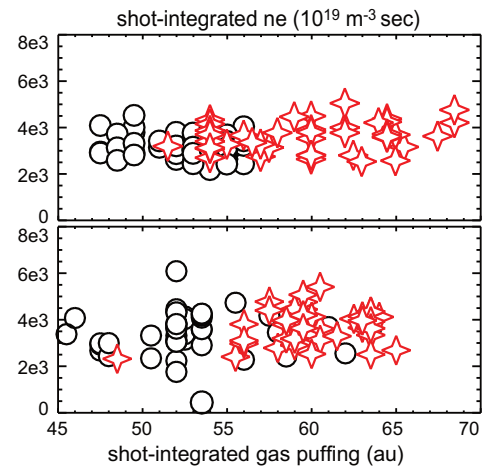


**Fig. 8.** Flattop-integrated  $n_e$  as a function of total puffing for the discharges before (circle) and after (star) boronizations on June 24, 2011 (top) and July 8, 2011 (bottom).

The reduction in the fuel recycling has also been implied after the boronization (and also after a subsequent overnight regular PDC session to remove the excessive hydrogen). This is shown in Fig. 8 where  $n_e$  integrated over an  $I_p$  flattop ( $\sim 20$  ms) during a shot as a function of the total fuel gas puffing for that shot is compared for the pre- and post-boronization plasmas. As shown in the Figure, after the boronization, more gas puffing is required to maintain the plasma density similar to that of the pre-boronization plasmas. This effect has been observed in many other devices with low- $Z$  deposition on the wall such as boronization [5] and often lithization [14].

Besides the effects on the reduction in the impurity content and fuel recycling, the boronization appears to allow MST to make prompt recovery from (both intended and accidental) vacuum vents. After a vent, MST usually follows its vacuum conditioning protocol aiming at ‘research-grade’ RFP discharges which specifically mean clean, reproducible, full-length flattop 500 kA RFP plasmas with normal gas puffing throughout the shot. In each phase, guidelines are given for operation parameters such as capacitor bank settings and phase-specific target plasma conditions which have to be achieved in order to go into the next phases. Based on many tests and subsequent modifications, the protocol estimates that the whole conditioning typically takes several weeks to complete and indeed it had been so during the pre-boronization ‘era’ (until the end of 2010). Since its first gaseous boronization in 2010, the vent recovery has taken only a couple of days or less, which significantly saves plasma run days. It seems that the boron film with oxygen on the wall is suspected to prevent, or slow down, the formation of water during the exposure to atmosphere.

#### 4. Summary and discussion

50 to 300 nm a-B/C:H coating has been formed using the o-carborane sublimation under pulsed discharge cleaning for the first time and has been seen to improve performance of MST RFP plasmas. A strong toroidal non-uniformity has been observed depending on the location of the source, implying that multiple o-carborane injectors will enable MST to obtain about 600–750 nm uniform coatings under the current PDC configuration (1 Hz,  $I_p = 10$ –15 kA) and with the current o-carborane loading (6–7 g per oven). The coating being much thicker than expected based on the PDC duty cycle is thought to be due to the long residence time of the o-carborane molecules, resulting in about 40% fuel utilization. Tests with further reduction in the number of the

PDC capacitors are underway, which is expected to reduce the PDC repetition time further and therefore to increase the o-carborane fuel efficiency. The downside of this path is that the reduced number of PDC capacitors would limit operation to lower plasma currents. However, it appears that it may be possible to reduce the present operating current,  $I_p = 10$  kA, further without negatively affecting performance.

The decrease in impurity content, or  $Z_{\text{eff}}$ , indirectly inferred from the X-ray spectra, is observed in RFP plasmas after the boronization although radiation from low-charge-state impurities measured by IMA only shows a marginally noticeable reduction during the magnetic reconnection events. This inference, however, assumes the same temperature and density between the pre- and post-boronization discharges. The assumption of constant temperature is questionable without measurements. It is also possible that good boronization improves the energy confinement thus increasing the temperature in the plasmas. In this case, a caution should be taken in comparing the offsets in the X-ray spectra to deduce  $Z_{\text{eff}}$  and a full numerical calculation should be performed.

The reduction in fuel recycling is consistently observed in most of the boronizations. This is inferred from the qualitative observation that more fuel puffing is necessary after to maintain the same plasma density as before the boronization. More solid and quantitative conclusions can be drawn by analyzing the coupons with thermal desorption spectroscopy (TDS) or nuclear reaction analysis (NRA) to measure exactly the amount of the hydrogen and deuterium in the deposition. So far, the coupons at MST have been dedicated to the XPS, ellipsometer, and profilometer – mostly for the measurements of the thickness, concentrations of the elements with  $Z > 2$  and hardness. Now that it is considered that this kind of information is reasonably reproducible, the material analysis will be focused more on the retention study using TDS and NRA.

Finally, one caveat in analyzing the coupons to characterize the quality of the deposition made inside the MST vessel is the significant difference in surface condition between the real MST wall and the Si coupons analyzed by the instruments. A recent inspection reveals that the MST wall is extremely rough (of the order of a millimeter) and porous after more than 20 years of plasma operations

whereas the roughness of the coupon is close to that of the Si wafer in the semiconductor industry ( $\sim 20$  nm). Therefore, the effects on the plasma performance might be different from what one expects from the thick and hard coating observed on the coupon and this may be what we have been observing in the MST plasmas after the boronization.

### Acknowledgements

The authors thank F.L. Tabarés and F.S.B. Anderson for their valuable comments on the development of the boronization system at MST. This work was supported by the United States Department of Energy.

### References

- [1] J. Winter, Plasma Phys. Control. Fusion 38 (1996) 1503–1542.
- [2] J. Winter, H.G. Esser, L. Konen, V. Philipps, H. Reimer, J.V. Seggaern, J. Schluter, E. Vietzke, F. Waelbroeck, P. Wienhold, T. Banno, D. Ringer, S. Veprek, J. Nucl. Mater. 162–164 (1989) 713–723.
- [3] P. Sonato, V. Antoni, W.R. Baker, R. Bertoncello, A. Buffa, L. Carraro, S. Costa, G.D. Mea, L. Marrelli, A. Murari, M.E. Puiatti, V. Rigato, P. Scarin, L. Tramontin, M. Valisa, S. Zandolin, J. Nucl. Mater. 227 (1996) 259–265.
- [4] T. Nakano, S. Higashijima, H. Kubo, J. Yagyu, T. Arai, N. Asakura, K. Itami, J. Nucl. Mater. 313–316 (2003) 149–152.
- [5] D. Tafalla, F.L. Tabarés, Vacuum 67 (2002) 393–397.
- [6] H.Y. Wang, X.M. Wang, J.H. Wu, J.H. Li, Y.W. Yu, Y. Yang, J. Phys.: Conf. Ser. 100 (2008) 062011.
- [7] S.H. Hong, K.S. Lee, K.M. Kim, H.T. Kim, G.P. Kim, J.H. Sun, H.J. Woo, J.M. Park, W.C. Kim, H.K. Kim, K.R. Park, H.L. Yang, H.K. Na, K.S. Chung, KSTAR team, Fusion Eng. Des. 85 (2010) 946–949.
- [8] L. Oren, R.J. Taylor, Nucl. Fus. 17 (1977) 1143–1151.
- [9] F.S.B. Anderson, Private Commun. (2010).
- [10] D.J. Den Hartog, M. Cekic, G. Fiksel, S.A. Hokin, R.D. Kendrick, S.C. Prager, M.R. Stoneking, J. Nucl. Mater. 200 (1993) 177–183.
- [11] D.J. Den Hartog, R.D. Kendrick, J. Nucl. Mater. 220–222 (1995) 631–635.
- [12] S. Ortolani, D.D. Schnack, Magnetohydrodynamics of Plasma Relaxation, World Scientific, 1993.
- [13] D.J. Clayton, A.F. Almagri, D.R. Burke, C.B. Forest, J.A. Goetz, M.C. Kaufman, R. O'Connell, Rev. Sci. Instrum. 81 (2010) 10E308.
- [14] F.L. Tabarés, M.A. Ochando, F. Medina, D. Tafalla, J.A. Ferreira, E. Ascibar, R. Balbín, T. Estrada, C. Fuentes, I. García-Cortés, J. Guasp, M. Liniers, I. Pastor, M.A. Pedrosa, The TJ-II Team, Plasma Phys. Control. Fusion 50 (2008) 124051.